Optimal topology and experimental evaluation of PE materials for actively shunted GE polymer matrix fiber composite blades

Benjamin Choi
NASA Glenn Research Center

Kirsten Duffy
The University of Toledo

Jeffrey Kauffman
The Pennsylvania State University

Nicholas Kray
GE Aviation

Objective

Investigate the feasibility of using piezoelectric sensors/actuators for subscale GEnx composite fan blade damping at target modes.

Outline

1. Introduction and literature survey
2. Passive shunt damping
3. Digital shunt control design and simulation results
4. Experimental evaluation of PE materials
5. Optimal topology for spin test
6. Spin test in GRC's Dynamic Spin Rig
7. Summary and future works

1. Introduction

Previous Activities at GRC

- Investigated several damping technologies to reduce excessive vibratory stresses that lead to high cycle fatigue (HCF) failures in aircraft engine turbomachinery.
- Developed viscoelastic damping, passive impact damping, plasma sprayed damping coating, and high temperature shape memory alloy (HTSMA).

Current Efforts at GRC

Develop a new damping technology for composite fan blades for future aircraft design in support of a Space Act Agreement with GE and as part of SFW project.

Proposed piezoelectric blade damping as a means of reducing engine blade vibration to support part of the project's goals.

- Demonstrated *RC* shunt damping of Ti-alloyed flat plates in GRC's Dynamic Spin Rig (K. Duffy and A. Provenza).
- Developed a digital shunt control that replaces equivalent passive-shunt analog circuits with a digital code. (B. Choi).
- In collaboration with MESA, developed a prototype of power transfer device that transmits control power to the PE actuators in the rotating frame (C. Morrison).
- Developed an FEM model to predict the system performance (J. Min).

Smart Fan Blade Technology Pros and Cons

- Benefits/Payoffs: support the NASA missions
  - Thinner and more efficient blades with shunt damping – fuel burn reduction, noise reduction, HCF failure reduction, etc.
  - Actively controlled blades - real-time health monitoring, aeroelastic control, mistuning problem, active fan distortion control for distributed propulsion system, etc.

- Drawbacks: structural characteristics degradation, durability and safety issues, added electronics weights, etc.
  - S. Mall (2002) investigated the integrity of the embedded active PZT sensor/actuator under monotonic and fatigue loads.
  - R. Pickering and K. Barlow (2007) specified the duration (10e+07 cycles) for each vibration mode for durability spin test.
  - Completed a preliminary durability bench test for 10^9 cycles under *4.6g* at target frequency. Need retest at high speed rotor.
  - On-going system trade study of blade weights reduction vs. added electronics weights.

Recent Advances in Turbomachinery Applications

1. Analog Shunt Circuits

- Passive control of turbomachine blading flow-induced vibrations (C. Cross, 2002).
- Passive shunt circuit was tested for piezoblade damping (S. Livet, 2008).
- Numerous papers published for passive shunt for rotorcraft vibration control.

➔ Most of them used a synthetic (or virtual) inductor that consists of op amps, resistors, capacitors, and ext. power supply

2. Active Control using Conventional PD Control Law

- Cascade flutter control using PE device in subsonic flow (T. Watanabe, 2005).
- Low-speed fan noise control using PE actuators mounted on stator vanes (P. Remington, 2003).
- Force excitation control using surface-mounted PE patches on the rotating blades (I. Santos, 2009).
  - First demo in the spin pit.
- NASA Ames/Boeing developed shape-shifting helicopter blades (2009). PE actuators created a mechanical motion that moves a flap up and down.

➔ Obviated a controversial issue concerning the use of PE.

Motivated us to continue the high-speed fan blade damping.

Full-scale helicopter smart blade in a Ames Res. Ctr. wind tunnel

Problems Using Conventional Methods

1) Analog circuits may not be viable for the rotating engine blades.
   - Impossible to accommodate the analog circuit size in the limited space
   - Possible to have the risk of rotor imbalance at high centrifugal loads
   - Hard to implement adaptive feature to follow changes in the blade's natural frequency
2) Active control using PD algorithm is not effective for resonant damping.

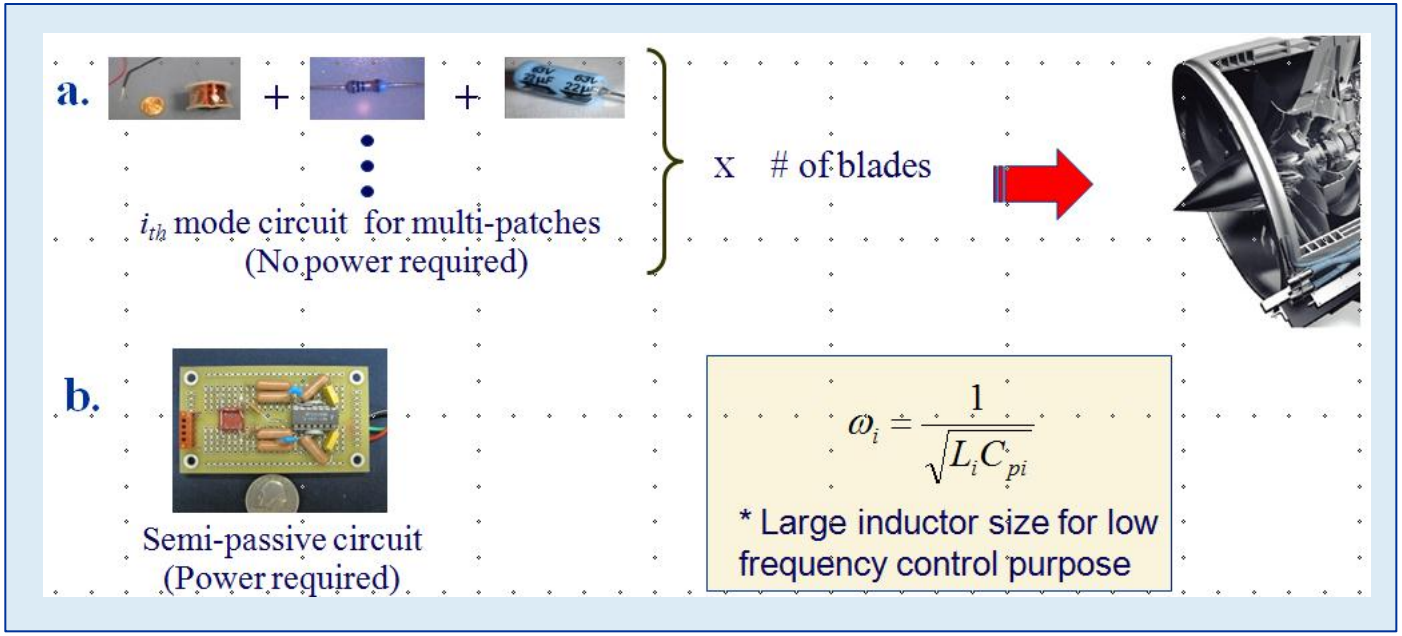

In this presentation

1. Active Shunt Control

- Replaces equivalent passive-shunt analog circuits with a digital code.
- Generates a real-time adaptive controller tuning to the changing condition of dynamic spin testing.
- Can be effective for multi-mode control because a few coding lines are necessary, as opposed to analog circuit approach.

2. Optimal Patch Selection

- Being tested/selected the best performing piezoelectric patches from several commercially available off-the-shelf piezoelectric materials.

3. Optimal Topology for GEnx Composite Blade

4. Initial Spin Test Result

3. Digital Control Design

Transfer Function of Analog *RLC* Circuit

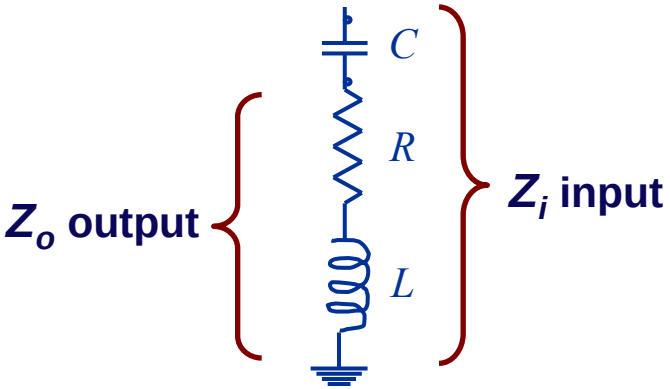

General feedback control *RLC* network.

$$Z_i = R + i\omega L - i/(\omega C)$$

$$Z_o = R + i\omega L$$

$$\frac{V_o}{V_i} = \frac{Z_o}{Z_i}$$

$$= \frac{R + i\omega L}{R + i\omega L - i/(\omega C)}$$

$$= \frac{Cs(R + Ls)}{LCs^2 + CRs + 1}$$

Expressed in terms of passive circuit components (***RLC***), regardless of modal shape.

TF of PID (proportional-integral-derivative) Control

$$G(s) = K_p + K_i / s + K_d s = (K_d s^2 + K_p s + K_i)/s$$

K_p: proportional gain, K_i: integral gain, K_d: derivative gain

Digital Control Design *(continued)*

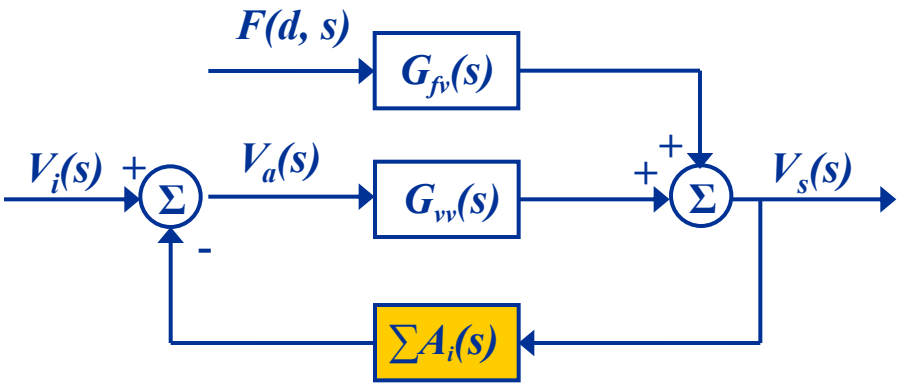

Fig. 1. Feedback control block diagram for blade structure with PEs.

The actuator voltage $V_a(s)$ is

$$V_a(s) = -A_i(s)V_s(s) + V_i(s)$$

where $A_i(s)$ is

$$A_i(s) = \frac{Cs(R_i + L_i s)}{L_i C s^2 + CR_i s + 1}$$

➢ A set of control laws in parallel circuits can be summed to control several modes (B. Choi, 2009).

The Closed-loop System Transfer Functions

$$V_s(s) = \frac{G_{fv}(s)F(d,s)}{1 + A(s)G_{vv}(s)} + \frac{G_{vv}(s)V_i(s)}{1 + A(s)G_{vv}(s)}$$

$$Y(r,s) = \frac{G_{fy}(r,s)F(d,s)}{1 + A(s)G_{vv}(s)} + \frac{G_{vy}(r,s)V_i(s)}{1 + A(s)G_{vv}(s)}$$

where

$$G_{fv}(s) = \frac{V_a(s)}{F(d,s)}, G_{vv}(s) = \frac{V_s(s)}{V_a(s)}$$

$$G_{fy}(r,s) = \frac{Y(r,s)}{F(d,s)}, G_{vy}(s) = \frac{Y(r,s)}{V_a(s)}$$

3.3 Simulation Results

- Constructed a six-mode truncated mathematical model, assuming ω_i and ζ_i

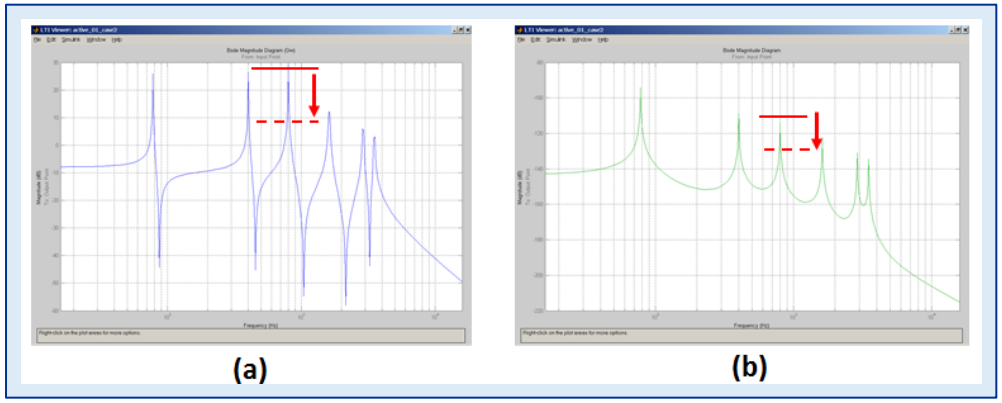

Figure 2. Open-loop frequency response of (a) G_{vv} and (b) G_{vy}.

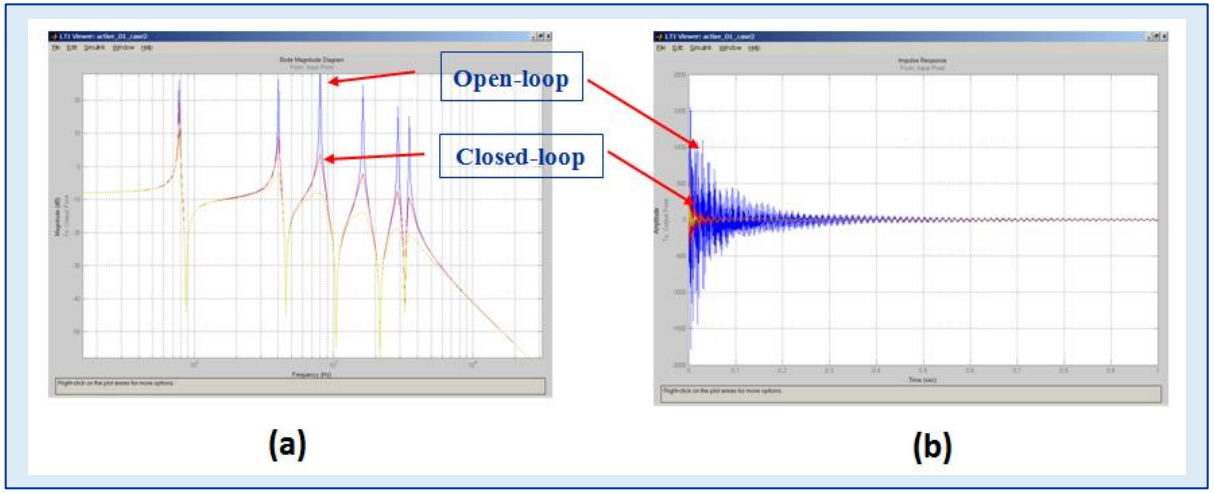

Figure 3. Open- and closed-loop frequency response of (a) G_{vv} and (b) Impulsive response of G_{vv}.

How To Implement Digital Control On The Rotating Fan Blades

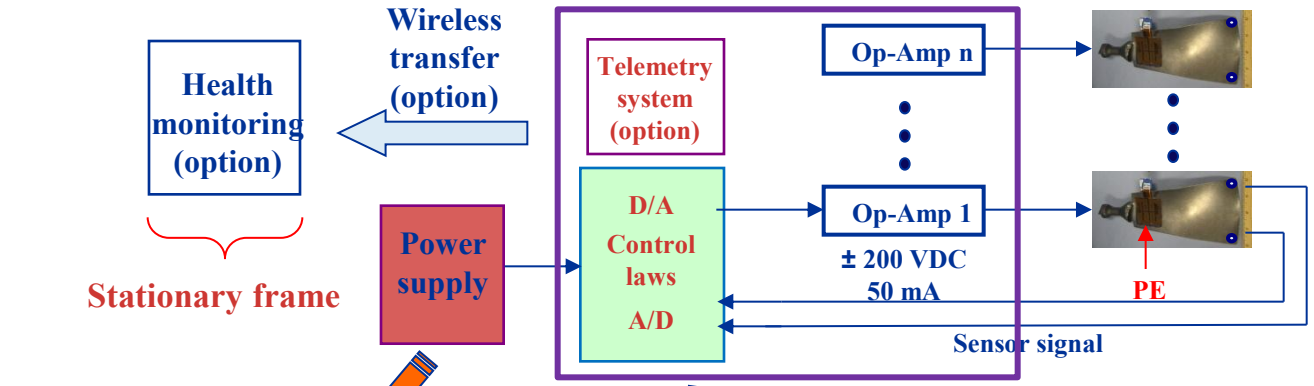

Photo courtesy of Datatel Telemetry
Inductively powered transmitter

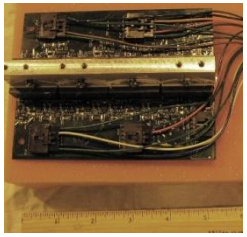

NASA GRC/MESA prototype control board w/ telemetry sys

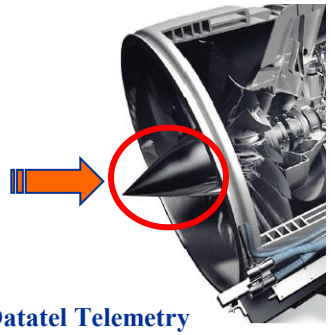

Photo courtesy of Datatel Telemetry

NASA GRC/MESA Control and Telemetry System

- Contains 8 inputs and 8 outputs, 8 Op-Amps (±200VDC @ 50mA), transmitter, and receiver. D/A card weighs about 0.3 lbs excluding its heat sink & supporting Aluminum block (0.2 lbs). A/D card weighs little less than 0.3 lbs.
- Adding more features into the controller block, its application will be further extended to health monitoring, aeroelastic control, mistuning problem, etc.
- Time lag of 1.5ms each path across the gap (“latency” in wireless transfer) makes difficult to move the controller to the stationary frame for the spin test purpose.

3.4 Experimental Bench Test Setup

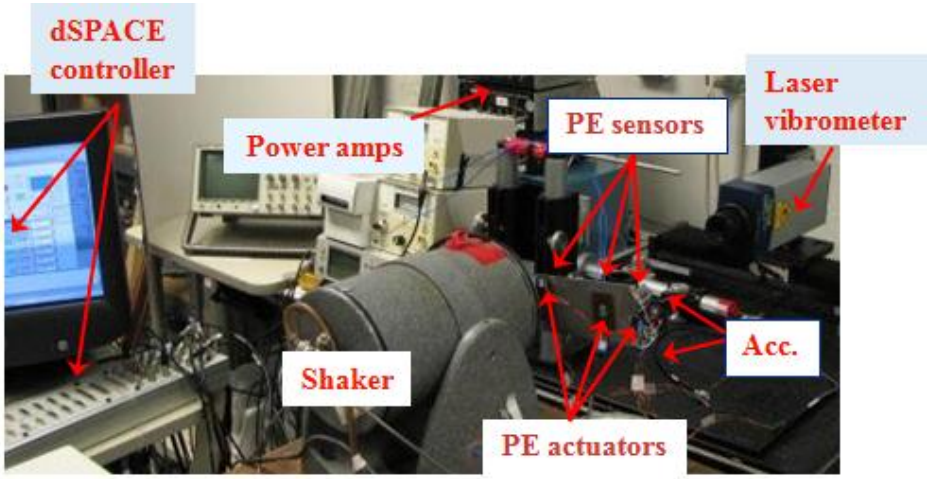

Figure 4. Experimental test setup.

- MATLAB/Simulink and the Real Time Workshop were used to generate C code for the digital shunt control laws, and the executable control code was downloaded into the dSPACE control system to implement the digital shunt.
- The acc. signal of the tip displacement was fed back to the dSPACE control system that generated the control command signal. The power amplifier magnified the signal and delivered power to energize the piezoelectric patches on the test specimen.
- Measured the open- and closed-loop transfer functions of the tip response to that of the base acc, and calculated the active damping performance.
- Here, the value for *L* was chosen to target a particular frequency, and the value for *R* was chosen to optimize the damping over the target frequency band.

4. Experimental Evaluation of PE Materials

- Investigate the ability, and effectiveness of using PE materials to damp resonant vibrations of GE-made composite coupons.
- Determine which type of PE patch generates the best performance in terms of damping and control power consumption.

Patches	Type	Dimension	Capacitance	V_{max}	F_{max}
MIDE QP10w	Flat, d_{31}	1.81" x 1.310" x 0.010"	*105 μF*	±200V	15 lbf
S-M M2814-P1	Flex, d_{33}	1.10" x 0.600" x 0.012"	*0.61 μF*	-500 to 1500V	195 lbf
S-M M2814-P2	Flex, d_{31}	1.10" x 0.600" x 0.012"	*25.7 μF*	-60 to 360V	85 lbf
S-M M0714-P2	Flex, d_{31}	0.275" x 0.30" x 0.012"	*6.5 μF*	-60 to 360V	85 lbf
Adv. Cerametrics	Flex, d_{33}	0.275" x 0.27" x N/A	*0.95 μF*	-60 to 360V	N/A

Table 1. Material properties of piezoelectric patches.

- PE patches were tested on the two polymer matrix fiber composite (PMFC) coupons: narrow and wide cantilever composite beams.
- Narrow beam: 9.5" x 1.3" x 0.25"; Wide beam: 9.5" x 2.0" x 0.25"

Experimental Evaluation of PE Material *(continued)*

- Begun bench testing the Advanced Cerametrics d_{33}-type vs. S-M d_{33}-type
- Targeted the 1st bending mode around 162.5 Hz.
- Generated a swept sine signal that was used to excite the beam through the target mode, and measured open- and closed-loop transfer functions.

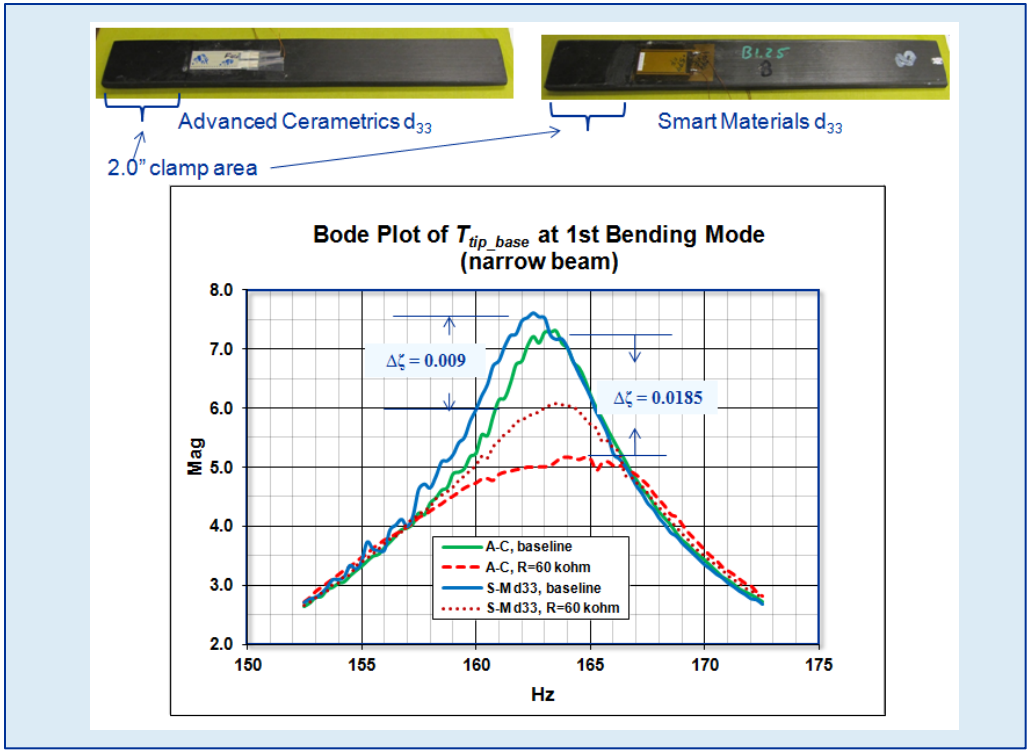

Figure 5. Bode plot of transfer functions around 1st bending mode

- With the same controller setup, the A-C d_{33}-type patch produced $\Delta\zeta = 0.0185$, while the Smart Material d_{33}-type produced $\Delta\zeta = 0.009$.

Experimental Evaluation of PE Material *(continued)*

- Another factor in determining the best performing patch candidate, is the required control power consumption for the added damping performance

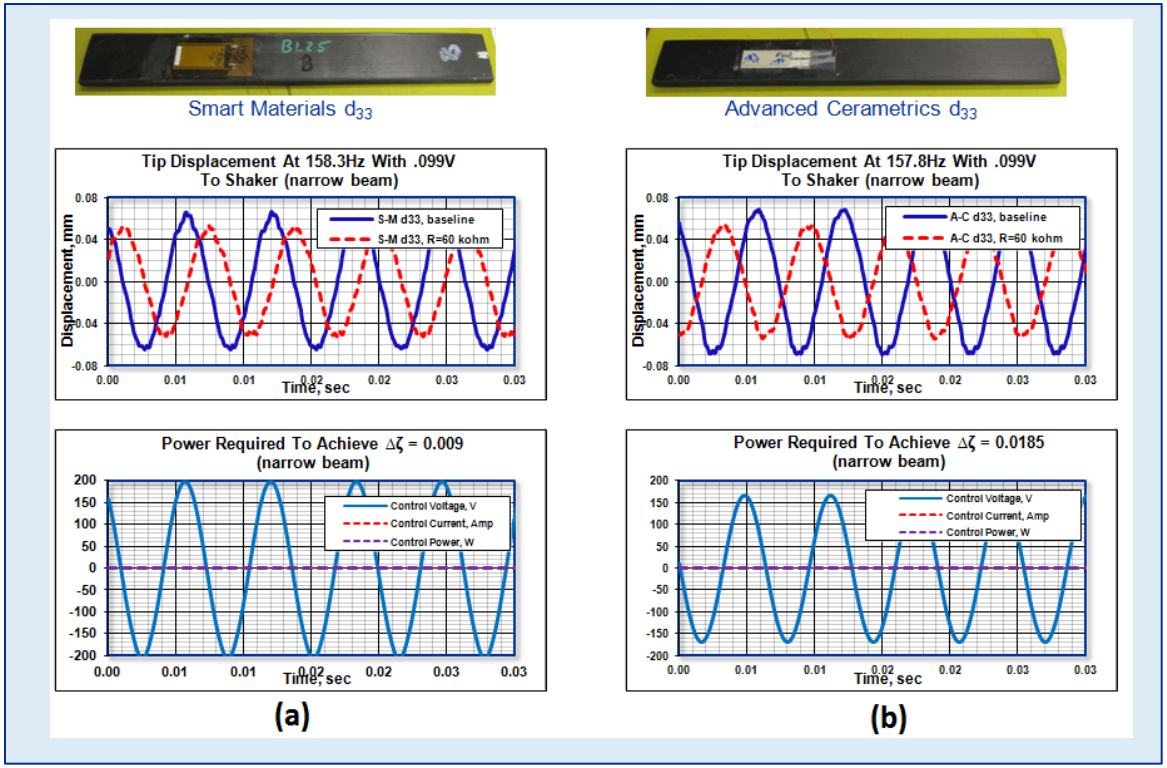

Figure 6. Control power consumption plots of using (a) S-M and (b) A-C

- A-C d_{33} type patch, consumed 0.185 *W* to perform $\Delta\zeta = 0.0185$, while the S-M d_{33}-type consumed 0.93 *W* to perform $\Delta\zeta = 0.009$.
- A-C actuator capability outperformed the S-M patch in terms of the damping and associated power efficiency.

Experimental Evaluation of PE Material *(continued)*

- Similarly, all other type patches were tested on the same narrow and/or other wide beams. All test results are summarized at Table 2.

Beam Type	PE Type	Piezoelectric Actuator	Damping Increase, $\Delta\xi$
Wide Beam	Non-flexible	Midé qp10n d_{31}	0.005
Wide Beam	Non-flexible	Midé qp10w d_{31} (wide)	0.001
Wide Beam	Flexible	Smart-Material d_{31}	0.012
Wide Beam	Flexible	Smart-Material d_{33}	0.007
Narrow Beam	Flexible	Smart-Material d_{31}	0.012
Narrow Beam	Flexible	Smart-Material d_{33}	0.009
Narrow Beam	Flexible	Advanced Cerametrics d_{33}	0.019

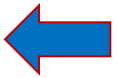

Table 2. Active damping increase results using different type piezoelectric patches.

- The best performing patch was the A-C d_{33}-type, but the correct size patch was not available.
- Thus, the second best **S-M d_{31}-type** was selected for the subscale GEnx blade damping work.

4.3 Non-rotating Testing of Subscale GEnx Blade

- Determine the actuation, sensing, and vibration damping capabilities of the S-M d_{31}-type patches.
- Obtain the modal stress of the target 1st bending mode at 0 rpm.
- Surface mount because the blade thickness was too small to contain the patches.

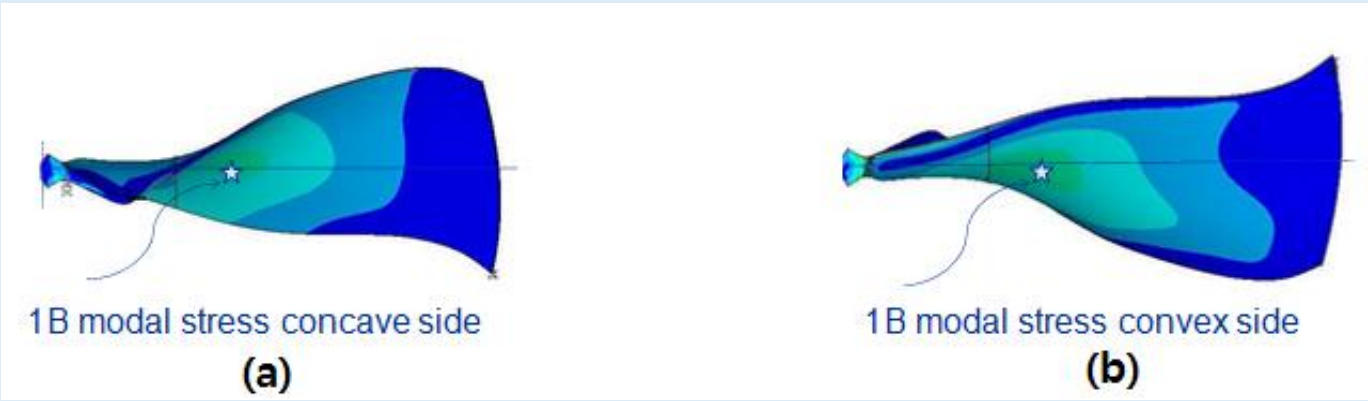

Figure 7. FEM analysis showing optimal patch locations for the target 1st bending mode.

- Decide on which side of the blade the PE actuator patch must be placed for better damping.
- Carry out several exp. tests to identify the optimal actuator and sensor patch configuration because no comprehensive FEM model of the GEnx blade with surface-mounted PEs was developed.

Non-rotating Testing of Subscale GEnx Blade *(continued)*

- Begun Test 1, where a S-M actuator (PE A) is placed on the convex side, and another S-M sensor patch (PE B) is placed on the concave side.
- Used additional acc. Signal feedback to confirm the accuracy and validity of the sensor patch functionality.

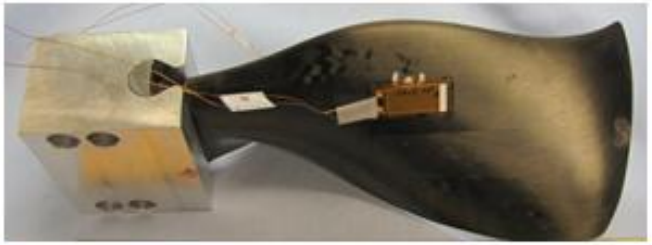

S-M d_{31} (*PE A*) actuator on the convex side **(a)**

S-M d_{31} (*PE B*) sensor and accelerometer on the concave side **(b)**

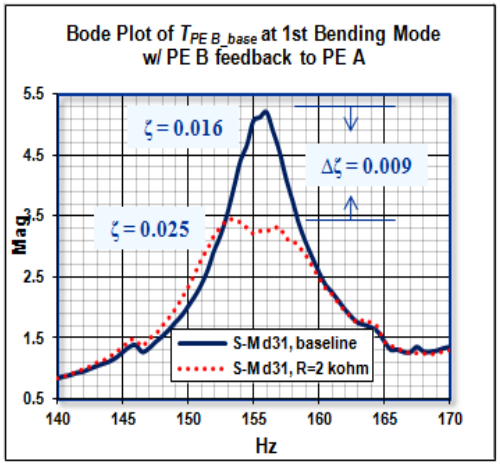

(a)

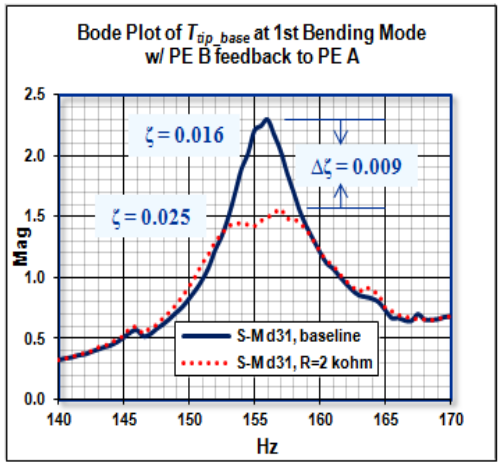

(b)

- $TF_{PEB\text{-}base}$, was taken, and $\Delta\zeta$ = 0.009.
- For comparison purpose, $TF_{tip\text{-}base}$, was taken, and $\Delta\zeta$ = 0.009.

Figure 9. Bode plot of transfer functions around 1st bending mode for the Test 1.

Non-rotating Testing of Subscale GEnx Blade *(continued)*

- Similarly, all other configurations were tested and evaluated by the blade tip damping and the PE sensor strain reduction.
- All exp. Resting results are summarized at Table 3.

Tests	Feedback sensor	Actuator	*TF* of the tip to the base, TF_{tip_base}	*TF* of the sensor PE to the base, TF_{PE_base}
Test 1	Piezo - Concave	Piezo - Convex	$\Delta\xi = 0.009$	$\Delta\xi = 0.009$
Test 2	Acc. - Concave	Piezo - Convex	$\Delta\xi = 0.011$	$\Delta\xi = 0.011$
Test 3	Acc. - Convex	Piezo - Concave	$\Delta\xi = 0.011$	$\Delta\xi = 0.009$
Test 4	Piezo - Convex	Piezo - Concave	$\Delta\xi = 0.021$	$\Delta\xi = 0.019$

Table 3. Exp. Results of increase in damping ratio using different patch configuration.

- Test 4 produced the best damping performance of $\Delta\zeta = 0.021$ from the TF_{tip_base}, and $\Delta\zeta = 0.019$ from the TF_{PEB_base}, respectively.
- Thus, we decided to place the actuator patch on the concave side, and to utilize a small sensing patch on the convex side for the ultimate goal of dynamic spinning test.

5. Optimal Topology for Spin Test

5.1 Single patch configuration

- Recent FEM analysis shows that the strain level on the convex side of the GEnx blade exceeds the PE patch's durable strain limit for high rotor speed.
- Thus, the previous Test 4 configuration is no longer viable, and all PEs must be located in the vicinity of the target placement on the concave side.

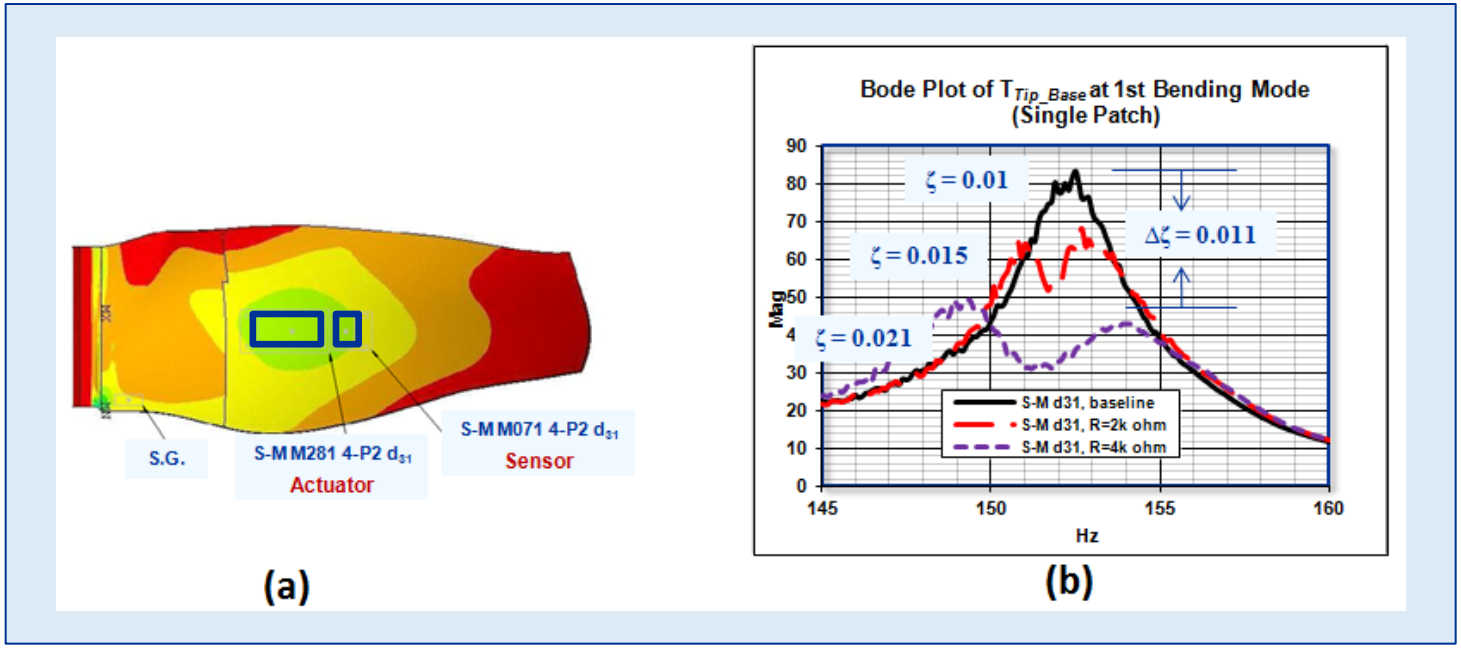

Figure 10. Actuator and sensor locations at the highest strain area. (b) Bode plot of TF_{Tip_Base}

- In this test setup, $\Delta\zeta = 0.011$ was achieved.

5.2 Double patch configuration

- A unique double patch configuration was proposed as one of the optimal topologies.
- Two large actuator patches and one small sensor patch are placed around the high modal strain location on the concave side.
- The two large patches can be energized simultaneously to increase the actuating power, or only one actuator can be used at a time, while the other can function as a backup in the event of actuation patch failure

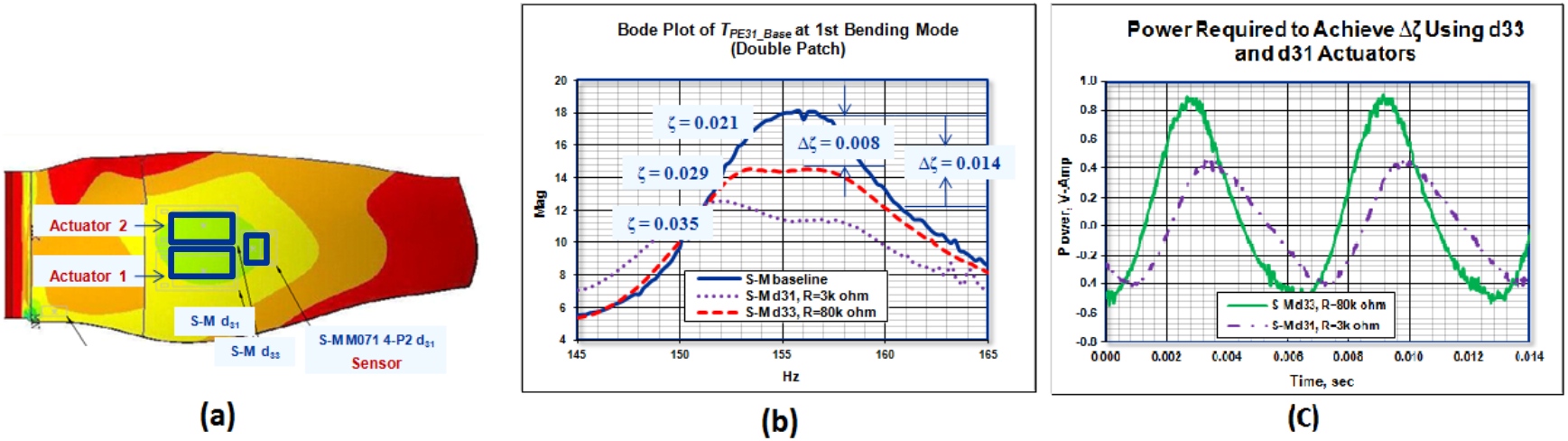

Figure 11. (a) Two actuators and one sensor (b) Bode plot of transfer functions, TF_{PE31_Base}, around 1st bending mode, (c) Control power consumption.

- d_{31}-type: 0.82 V-Amp to achieve $\Delta\zeta = 0.014$; d_{33}-type: 1.34 V-Amp to achieve $\Delta\zeta = 0.008$.
- Concluded that **the optimal topology of the spin test** is the double patch configuration with two big S-M d_{31}-type actuators and one small S-M d_{31}-type sensor patch, all bonded on the concave side.

6. Spin Test Results

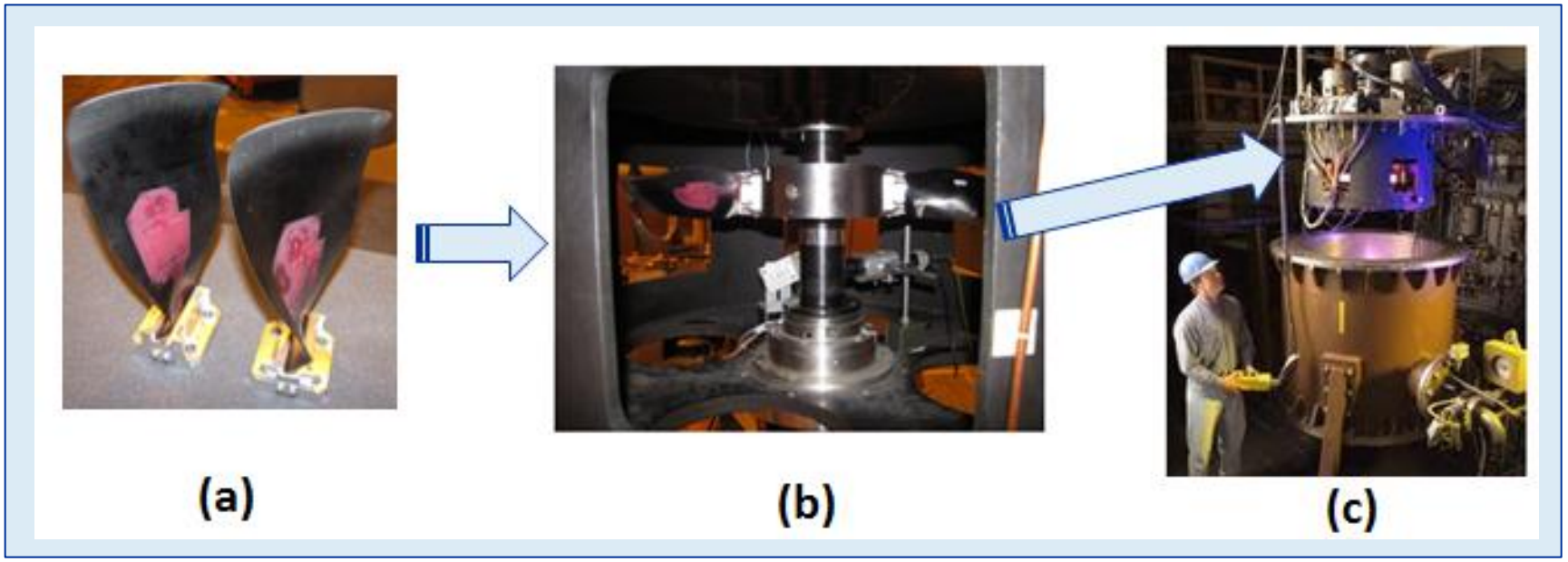

Figure 12. Blades in the GRC's Dynamic Spin Rig.

- GE Aviation instrumented two test blades with the double patch configuration.
- The two blades were fixed to a vertical rotor, and the rotor was placed in a vacuum tank during operation.
- Excitation was provided to the blades through the magnetic bearings that levitated the rotor and blades in five axes.
- As the shaft rotational speed changes, the blade's natural frequencies will vary due to centrifugal loads. Thus, an adaptive control feature was added to the closed-loop controller using a lookup table method.

Spin Test Results *(continued)*

- The blades have slightly different resonance frequencies, and coupling exists between the blades through the rotor, resulting in each blade exhibiting two peaks.
- The test was done using Blade 2 that has the higher response.

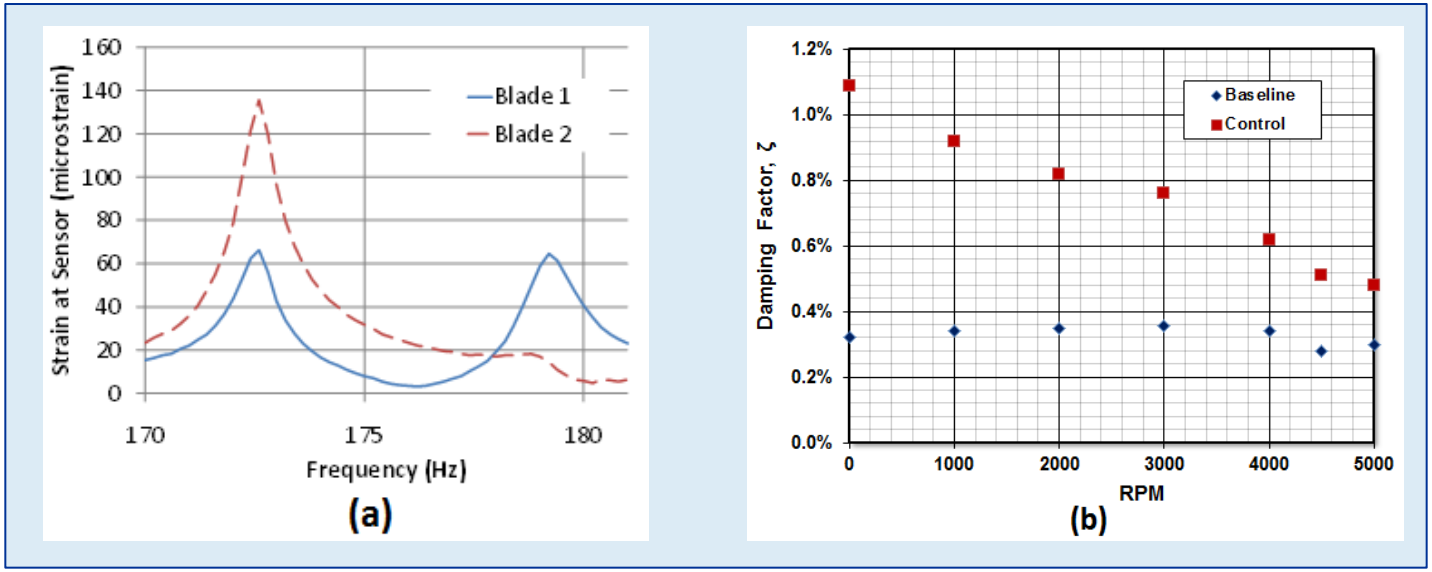

Figure 13. (a) First bending resonant peaks[18] at 0 rpm, (b) Damping ratio for baseline open circuit and actively controlled blades.

- Ran the spin test and measured open- and closed-loop transfer functions.
- Achieved significant blade damping at 0 rpm, but the ability to damp decreased as the rotor speed increased. Caused by the blade's centrifugal stiffening and by the peak modal strain location changing with the rotor speed.

- A more detailed discussion will be published in a subsequent paper[18]

7. Conclusion

- ✓ An **active shunt control** technique that emulated the tuned RLC circuit was developed, enabling our team to accomplish a GRC Center milestone of demonstrating blade damping in a spin test.
- ✓ Several commercially available off-the-shelf piezoelectric materials were tested through a series of the bench top tests. They were evaluated in terms of damping capability and associated control power requirement, and the Smart Material's d_{31}-type (**S-M M2814-P2**) was finally selected.
- ✓ We finalized the optimal patch topology of the GEnx fan blade with the **double-patch configuration**, where two identical S-M d_{31}-type actuator patches and one small S-M d_{31}-type sensor patch were placed around the high modal strain location on the concave (pressure) side.
- ✓ Finally, successful **spin testing** up to 5,000 rpm was done in GRC's Dynamic Spin Rig. If damping is required over a particular speed range, the actuator location(s) should be chosen based on high modal strain for that speed range of interest.

- ➢ There are definitely more challenging technical aspects that must be considered, and more research must be accomplished before implementing the piezoelectric damping control system.
- ➢ However, this paper is an attempt at **the initial task of proving the feasibility of blade damping**.